Study on Numerical Simulation and Experiment of Lightguide Plate in Injection Molding

Y. K. Shen, W. Y. Wu, S. Y. Yang, H. M. Jian and C -C. A. Chen

Journal of Reinforced Plastics and Composites 2004; 23; 1187
DOI: 10.1177/0731684404037040

Study on Numerical Simulation and Experiment of Lightguide Plate in Injection Molding

Y. K. SHEN* AND W. Y. WU
Department of Mechanical Engineering
Lunghwa University of Science and Technology
Taoyuan 333, Taiwan, ROC

S. Y. YANG AND H. M. JIAN
Department of Mechanical Engineering
National Taiwan University
Taipei 106, Taiwan, ROC

C-C. A. CHEN
Department of Mechanical Engineering
National Taiwan University of Science and Technology
Taipei 106, Taiwan, ROC

ABSTRACT: This paper presents the application of injection molding of wedge-shaped plates for lightguiding application. This paper discusses the influence of processing parameters on injection molding. The filling stages of lightguide plate for mold flow simulation (3D, midplane) are analyzed. The numerical simulation of mold filling process is based on the concept of control volume finite element method. The hot plastic melt touches the cold wall that forms the solid layer, a solid–liquid interface moves and a two-phase flow exists. The enthalpy model is used to predict this interface in the two-phase flow problem. The experiments carry out short-shots process to compare with numerical simulation. The experiments also indicate the pressure distribution at thin and thick ends of lightguide plate using pressure transducers. The results show that the results of 3D filling situation is close to those from experiments. The melt front progress of 3D numerical simulation is predicted more accurately than midplane numerical simulation.

KEY WORDS: lightguide plate, injection molding, finite element method, enthalpy model, flow visualization.

INTRODUCTION

THE APPLICATION OF 3C and optical product is more wide in the world. The shape and thickness of product changes more quickly these days.

The lightguide plate is the major part of liquid crystal display (LCD). Its function is transformation of the light of cold cathode fluorescernt lamp (CCFL) to face of liquid

*Author to whom correspondence should be addressed. E-mail: ykshen@mail.me.lhu.edu.tw

0731-6844/04/11 1187–20 $10.00/0 DOI: 10.1177/0731684404037040

crystal. Since the lightguide plate must introduce light uniformly, the scale quality and optical property is very important for lightguide plate.

The commercial CAE packages such as Cadmould, C-Mold and MoldFlow have become useful tools for mold design. These packages are based on the Hele-Shaw model in which two-dimensional elements are used to represent the thin shell geometry. The simulation method of these packages is named for midplane numerical simulation. The Hele-Shaw model neglects the inertia and the gap-wise velocity components for polymer melt flow in the thin cavities. The Hele-Shaw mold used in the flow regions i.e. flow around corners, or thickness-change regions, or the fountain flow effect of melt fronts cannot be represented in details. Only the 3D numerical simulation based on Navier–Stokes equation can simulate the reality situation.

Zachert and Michaeli [1] used the 3D simulation (MAGMAsoft) and two-dimensional simulation (CADMOULD-3D) to compare experiments with a special mold. In comparison to a regular two-dimensional simulation, the flow front progress of 3D simulation is predicted more accurately. Floryan and Rasmussen [2] reviewed the numerical algorithms for the analysis of viscous flows with moving interface. They discussed the available algorithms can be classified as Eulerian and Lagrangian. Eulerian algorithms consist of fixed grid method, adaptive grid method, mapping method, and special method. Lagrangian algorithms consist of strictly Lagrangian method, Lagrangian method with rezoning, free Lagrangian method, and particle method. Their paper dealt with moving boundary problems with small to medium deformations for former methods.

Shen and Wu [3] used the 3D numerical simulation (control volume finite element method) to simulate microgear for example. The analysis discussed with different polymer (PP, PA, POM) and process parameters (injection time, injection pressure, injection temperature, and mold temperature). The results showed that the mold temperature was the most important factor on process parameters. The mold temperature of micro-injection molding must be higher than the transition glass temperature of plastic material. The most suitable material was PP. Hetu et al. [4], which presented a 3D finite element model capable of predicting the velocity, pressure, and temperature fields as well as the position of the flow fronts. The tracking of the flow front was modeled by using a pseudo-concentration method and the model equations were solved using a Petrov–Galerkin formulation. The model predicted the physical phenomena such as fountain flow, a 1 : 4 expansion representative of 3D regions and an automotive door handle of a thick cross section. It performed equally well on these cases. Kabanemi et al. [5] described a fully 3D transient finite element method for calculating the flow behavior and fiber orientation during the injection molding of thick wall parts. The main result of this contribution was the natural way to treat singular regions such as the fountain flow and areas near the gate where the flow was fully 3D and kinematics effects were not instantaneous even in the case of the small thickness parts. The front region was not straight and therefore the Hele-Show approximations were not valid. Haagh and Vosse [6] developed the numerical model for both two- and 3D mold filling simulations. This paper employed a pesudo-concentration method in order to avoid elaborate 3D mesh and had been implemented in a finite element program. The moving contact line problem had been overcome by employing a Robin boundary condition at the mold walls, which can be turned into a biriohlet (no-slip) or a Neumann (free-ship) boundary condition depending on the local pesudo-concentration. The model presented on this paper had proven to work well for the filling of both two- and 3D molds: both the advancement of the flow front and fountain flow effect. Hwang and Kwon [7] developed the 3D finite element analysis system that used to simulate a filling

process of powder injection molding for general 3D parts. The good agreements between the experimentals and numerical results indicated that the melt front tracing scheme successfully simulates the transient filling process.

The purpose of this work is to model and simulate the flow characteristics of the lightguide plate on process by midplane and 3D simulation. This work uses former result to optimize mold design and operation. The enthalpy model is used to predict the solid–liquid interface of the two-phase flow for filling stage on 3D numerical simulation. This work observes the flow situation of lightguide plate for filling stage on experiment to compare the results with numerical simulation.

EXPERIMENT

This work uses the injection mold machine (SM-80) produced by Chen Hsong company (the clamp force is 80 tons). The material of experiment is used for PS material (886) by DELTA company. The properties of PS are shown in Table 1. The lightguide plate is the wedged-shape plate. The mold of wedged-shape plate is three-plate mold. The geometry of mold is shown on Figure 1. The details of three-plate mold are shown in Figure 2. The parameters of processing condition are listed in Table 2. This work measures the pressure distribution of cavity to compare the results of numerical simulation on the filling stage. The pressure transducer is bedded on mold surface for catching the pressure value of processing. The two pressure transducers (KISTLER 6159A) are bedded on the thick and thin end of the mold. The positions of pressure transducer are shown on Figure 1. The P1 pressure transducer is located on thick end and P2 is located on thin end of the mold. The pressure value was measured by pressure transducer that transforms to voltage value on processing. This voltage value is output by amplifier (Kistler 5041C). The computer reads the voltage value by A/D card and transforms the value to pressure versus time. The system of catching pressure distribution is shown in Figure 3.

Table 1. The properties of PS.

Parameter	Value
Liquid density (ρ_l, g/cm^3)	0.9686
Solid density (ρ_s, g/cm^3)	1.0685
Liquid thermal conductivity (W/m C)	0.173
Solid thermal conductivity (W/m C)	0.138
Liquid specific heat (J/kg C)	2545.5
Solid specific heat (J/kg C)	1552.5
n	0.3154
τ^* (Pa)	82999
D_1(Pa s)	2.119e + 011
D_2 (K)	373.15
D_3 (KPa)	0
A_1	26.8
A_2 (K)	51.6
T_{ref} (K)	298
T_m (K)	453
L (J/g)	135.3
H_{in} (J/g)	455.88
H_w (J/g)	23.53

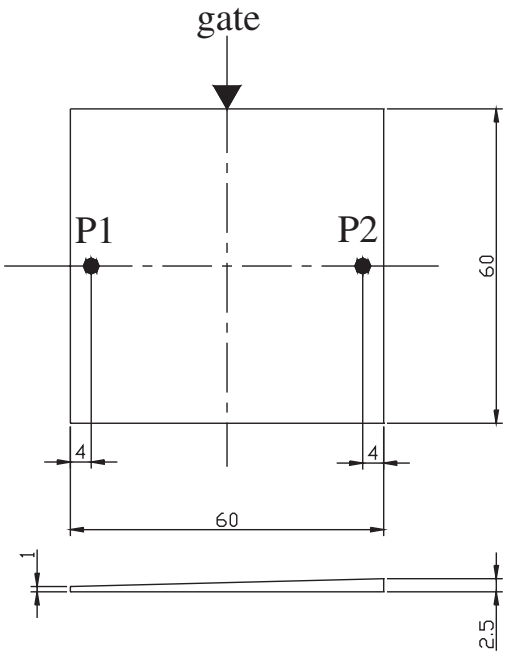

Figure 1. *The geometry of mold. (unit: mm), (P1, P2 is pressure transducer).*

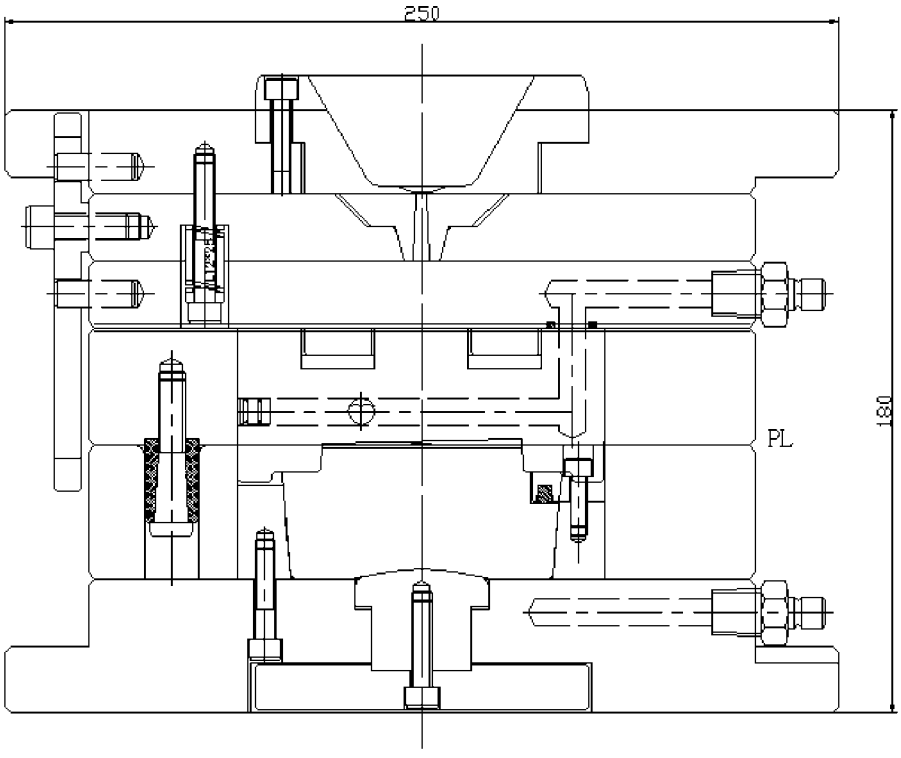

Figure 2. *The mold of wedge-shaped plates.*

Table 2. The parameters of processing condition.

Parameter Condition	Press Compression Force (%)	Press Compression Time (s)	Packing Pressure (%)	Packing Time (s)	Mold Temperature (°C)	Melt Temperature (°C)
1	10	1.0	5	0.5	40°C	210°C
2	30	2.0	10	1.0	60°C	230°C
3	50	4.0	15	1.5	80°C	250°C
4	70	6.0	20	2.0		
5	90	8.0				
6		10.0				
7		12.0				

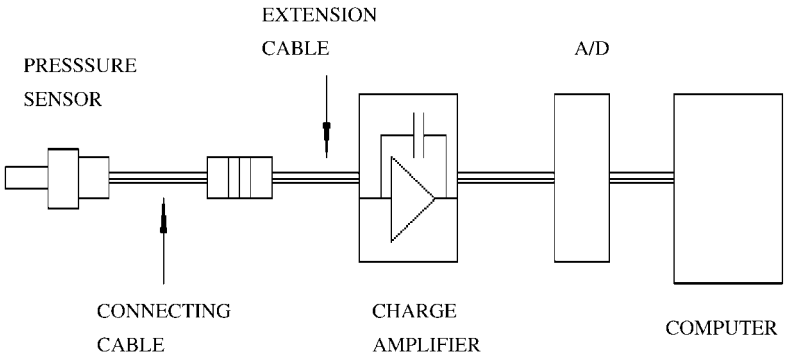

Figure 3. *Pressure value getting system.*

MATHEMATICAL MODEL

3D Model

The mass, momentum, and energy conversation governing equations for the non-isothermal, generalized Newtonian fluid are given by:

Continuity Equation:

$$\frac{\partial \rho}{\partial t} + \frac{\partial(\rho u)}{\partial x} + \frac{\partial(\rho v)}{\partial y} + \frac{\partial(\rho w)}{\partial z} = 0 \tag{1}$$

Momentum Equation:

$$\rho\left(\frac{\partial u}{\partial t} + u\frac{\partial u}{\partial x} + v\frac{\partial u}{\partial y} + w\frac{\partial u}{\partial z}\right) = -\frac{\partial p}{\partial x} + \eta\left(\frac{\partial^2 u}{\partial x^2} + \frac{\partial^2 u}{\partial y^2} + \frac{\partial^2 u}{\partial z^2}\right) + \rho g_x \tag{2}$$

$$\rho\left(\frac{\partial v}{\partial t} + u\frac{\partial v}{\partial x} + v\frac{\partial v}{\partial y} + w\frac{\partial v}{\partial z}\right) = -\frac{\partial p}{\partial y} + \eta\left(\frac{\partial^2 v}{\partial x^2} + \frac{\partial^2 v}{\partial y^2} + \frac{\partial^2 v}{\partial z^2}\right) + \rho g_y \tag{3}$$

$$\rho\left(\frac{\partial w}{\partial t}+u\frac{\partial w}{\partial x}+v\frac{\partial w}{\partial y}+w\frac{\partial w}{\partial z}\right)=-\frac{\partial p}{\partial z}+\eta\left(\frac{\partial^2 w}{\partial x^2}+\frac{\partial^2 w}{\partial y^2}+\frac{\partial^2 w}{\partial z^2}\right)+\rho g_z \tag{4}$$

Energy Equation:

$$\left(\frac{\partial H}{\partial t}+u\frac{\partial H}{\partial x}+v\frac{\partial H}{\partial y}+w\frac{\partial H}{\partial z}\right)=\alpha\left(\frac{\partial^2 H}{\partial x^2}+\frac{\partial^2 H}{\partial y^2}+\frac{\partial^2 H}{\partial z^2}\right)+\eta\dot{\gamma}^2 \tag{5}$$

$$\dot{\gamma}=\sqrt{\left(\frac{\partial u}{\partial x}\right)^2+\left(\frac{\partial v}{\partial y}\right)^2+\left(\frac{\partial w}{\partial z}\right)^2} \tag{6}$$

$$\alpha=\frac{\bar{k}}{\bar{\rho}\bar{c}_p},\quad \bar{k}=\frac{k_\mathrm{s}+k_\mathrm{l}}{2},\quad \bar{\rho}=\frac{\rho_\mathrm{s}+\rho_\mathrm{l}}{2},\quad \bar{\mathrm{c}}_p=\frac{\bar{c}_\mathrm{ps}+\bar{c}_\mathrm{pl}}{2} \tag{7}$$

where x, y, z is the Cartesian coordinate, t is the time, ρ_s, ρ_l is the solid, liquid density, u, v, w is the velocity, p is the pressure, g is the gravity, η is the viscosity, c_ps, c_pl is the solid, liquid specific heat, k_s, k_l is the solid, liquid thermal conductivity, H is the enthalpy and $\dot{\gamma}$ is the shear rate.

For the Stefan problem the enthalpy (H) is defined as (Figure 4) [8]

$$H=\rho_\mathrm{s}c_\mathrm{ps}(T-T_\mathrm{ref})+\int_0^{\mathrm{pl}}\left[\bar{v}_\mathrm{s}-T\left(\frac{\partial\bar{v}_\mathrm{s}}{\partial T}\right)_p\right]dp,\quad \text{for } T<T_m \tag{8}$$

$$H=\rho_\mathrm{s}c_\mathrm{ps}(T_m-T_\mathrm{ref})+\rho_\mathrm{s}L+\rho_\mathrm{l}c_\mathrm{pl}(T-T_m)+\int_0^{\mathrm{pl}}\left[\bar{v}_\mathrm{l}-T\left(\frac{\partial\bar{v}_l}{\partial T}\right)_p\right]dp,\quad \text{for } T\geq T_m \tag{9}$$

where $\bar{v}=$ volume/mole.

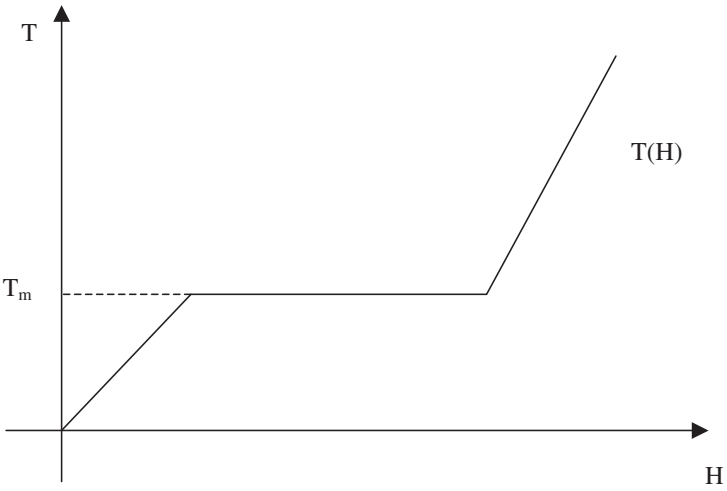

Figure 4. *The enthalpy function.*

The viscosity model of fluid:

$$\eta(\dot{\gamma}, T, P) = \frac{\eta_0(T, P)}{1 + (\eta_0 \dot{\gamma}/\tau^*)^{1-n}} \tag{10}$$

$$\eta_0(T, P) = D_1 \exp\left[-\frac{A_1(T - T*)}{A_2 + (T - T*)}\right] \quad T > T* \tag{11}$$
$$\eta_0(T, p) = \infty \qquad\qquad\qquad\qquad\quad T \leq T*$$

$$T^*(p) = D_2 + D_3 p \tag{12}$$

$$A_2 = \bar{A}_2 + D_3 p \tag{13}$$

where T^* is the glass-transition temperature, n is flow index.

Boundary and Initial Conditions:

$$u = v = w = 0\,; \quad H = H_w\,; \quad \frac{\partial p}{\partial n} = 0 \quad \text{at } z = \pm b \text{ (on mold wall)} \tag{14}$$

$$\frac{\partial u}{\partial z} = \frac{\partial v}{\partial z} = \frac{\partial w}{\partial z} = \frac{\partial H}{\partial z} = 0 \quad \text{at } z = 0 \text{ (on center line)} \tag{15}$$

$$p = 0 \text{ on melt front} \tag{16}$$

$$p = p_e(x, y, z, t) \text{ on inlet} \tag{17}$$

where H_W is the mold enthalpy, n is normal direction and P_e is the inlet pressure.

Hele-Shaw Model

The product of plastic part is assumed to the thin part. The model of flow field often uses Hele-Shaw model. The governing equations for the nonisothermal, generalized Newtonian fluid are given by:

Continuity Equation:

$$\frac{\partial \rho}{\partial t} + \frac{\partial(\rho u)}{\partial x} + \frac{\partial(\rho v)}{\partial y} + \frac{\partial(\rho w)}{\partial z} = 0 \tag{18}$$

Momentum Equation:

$$0 = \frac{\partial}{\partial z}\left(\eta \frac{\partial u}{\partial z}\right) - \frac{\partial p}{\partial x} \tag{19}$$

$$0 = \frac{\partial}{\partial z}\left(\eta \frac{\partial v}{\partial z}\right) - \frac{\partial p}{\partial y} \tag{20}$$

Energy Equation:

$$\rho c_p\left(\frac{\partial T}{\partial t}+u\frac{\partial T}{\partial x}+v\frac{\partial T}{\partial y}\right)=\frac{\partial}{\partial z}\left(k\frac{\partial T}{\partial z}\right)+\eta\dot{\gamma}^2 \tag{21}$$

$$\text{Then } \dot{\gamma}=\sqrt{\left(\frac{\partial u}{\partial x}\right)^2+\left(\frac{\partial v}{\partial y}\right)^2} \tag{22}$$

The viscosity model of fluid is the same as Equation (10)–(11).

Boundary and initial conditions:

$$u=v=0\,;\quad T=T_w\quad \text{at } z=\pm b \text{ (on mold wall)} \tag{23}$$

$$\frac{\partial u}{\partial z}=\frac{\partial v}{\partial z}=\frac{\partial T}{\partial z}=0\quad \text{at } z=0 \text{ (on center line)} \tag{24}$$

The pressure is independent of z-direction. The momentum Equation (19), (20) integrates to the following equations:

$$\eta\left(\frac{\partial u}{\partial z}\right)=\left(\frac{\partial p}{\partial x}\right)z \tag{25}$$

$$\eta\left(\frac{\partial v}{\partial z}\right)=\left(\frac{\partial p}{\partial y}\right)z \tag{26}$$

by the boundary condition, the Equation (25), (26):

$$u=\left(-\frac{\partial p}{\partial x}\right)\int_z^b\frac{z\,dz}{\eta} \tag{27}$$

$$v=\left(-\frac{\partial p}{\partial y}\right)\int_z^b\frac{z\,dz}{\eta} \tag{28}$$

Integrates the Equation (27), (28):

$$\overline{u}=\left(-\frac{\partial p}{\partial x}\right)\frac{S}{b} \tag{29}$$

$$\overline{v}=\left(-\frac{\partial p}{\partial y}\right)\frac{S}{b} \tag{30}$$

$$S=\int_0^b\rho\frac{z^2dz}{\eta} \tag{31}$$

where $\bar{u}$, $\bar{v}$ is the average velocity and S is the fluidity.

Equation (29), (30) adds to (18), then get

$$\frac{\partial}{\partial t}\int_0^h \rho dz - \frac{\partial}{\partial_x}\left(S\frac{\partial p}{\partial x}\right) - \frac{\partial}{\partial_y}\left(S\frac{\partial p}{\partial y}\right) = 0 \tag{32}$$

because $\rho = \rho\ (T,\ p)$

$$\frac{\partial}{\partial t}\int_0^h \rho dz = G\frac{\partial p}{\partial t} + F \tag{33}$$

$$G = \int_0^x \left(\frac{\partial \rho_l}{\partial p}\right)_T dz + \int_x^h \left(\frac{\partial \rho_s}{\partial p}\right)_T dz \tag{34}$$

$$F = \int_0^x \left(\frac{\partial \rho_l}{\partial T}\right)_p \frac{\partial T}{\partial t} dz + \int_x^h \left(\frac{\partial \rho_s}{\partial T}\right)_p \frac{\partial T}{\partial t} dz + (\rho_l - \rho_s)_{z=x}\frac{\partial x}{\partial t} \tag{35}$$

Where ρ_l is the liquid density and ρ_s is the solid density.

The boundary conditions for Equation (33) are:

$$p = 0 \text{ on melt front} \tag{36}$$

$$p = p_e(x, y, t) \text{ on inlet} \tag{37}$$

$$\frac{\partial p}{\partial n} = 0 \text{ on mold wall} \tag{38}$$

NUMERICAL METHODS

3D Numerical Simulation

The model has (a) five independent variables: three velocities (u, v, w), one pressure (p) and one enthalpy (H), (b) one dependent variable: viscosity(η).

In this paper, the work used the control volume finite element method to solve the governing equations. This paper uses the penalty function method to replace the pressure for reducing the independent variables.

$$P = -\lambda\left(\frac{\partial u}{\partial x} + \frac{\partial v}{\partial y} + \frac{\partial w}{\partial z}\right) \tag{39}$$

where λ is the penalty parameter. $\lambda = c \times n$, n is the fluid viscosity, c is concerned by the byte length of computer. In this paper, c is chosen by the 10^7 value for simulation.

for flow field

$$[M]\{\dot{U}\} + [K]\{U\} = \{F\} \tag{40}$$

where $\dot{U}$and U represent the acceleration and the velocity of finite element nodes. The matrix M is the mass matrix. K is the diffusion matrix and F is the force vector. K is composed of two parts: the viscosity term and the penalty term.

for thermal field

$$\left[M^H\right]\{\dot{H}\} + \left[K^H\right]\{H\} = \left\{F^H\right\} \tag{41}$$

where $\dot{H}$ and H represent the rate of enthalpy and enthalpy of finite element nodes. The matrix M^H is the mass matrix for enthalpy. K^H is the diffusion matrix for enthalpy and F^H is the force vector for dissipation.

The viscosity of melting polymer is highly dependent variable for temperature, the flow and heat transport equations are strongly coupled. The solution procedure follows the repeated sequence of (a) solving the flow field with given enthalpy H and (b) solving the thermal field with solved velocity u, v, and w.

Finite Element Implementation

A model of mixed finite element based on a four node tetrahedral Pl^+/Pl element has been shown on Figure 5.

The element, having a fifth node in its centroid, satisfies the Brezzi-Babuska conditions, which are necessary to ensure a stable solution for the Navier–Stokes equations using the Galerkin method.

For the given element, a fifth node at the centroid is used to construct the piecewise linear approximation (Pl^+) for the velocity field. This decomposes the element into four subtetrahedrons. The trial function for velocity is constituted by four linear components and a bubble function. The pressure is defined linearly using the four vertices. In this work, a bubble function being zero at the element boundary and piecewise linear on sub-tetrahedrons is chosen for the numerical integration.

Even though the centroid is used as a part of velocity field approximations when building the elementary matrices, it can be eliminated by the ''static condensation'' procedure at element level leading to the initial four node tetrahedrons.

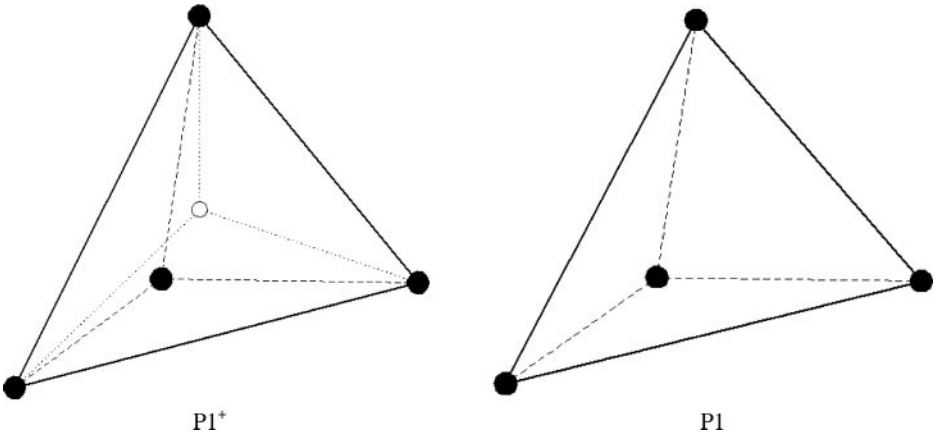

Figure 5. *The $P1^+/P1$ velocity–pressure element.*

The finite element discretization of the flow equations leads to a highly nonlinear system. Therefore the Newton–Raphson scheme is employed to linearize the equations.

Front Tracking Equation

The position of the moving interface can be modeled by various techniques, and several methods have been proposed in the last decade [2]. The tracking of the flow front in the mold cavity is modeled using VOF (Volume of Fluid) technique in this work [9]. Discretization of the 3D domain was done with a tetrahedron finite element (see Figure 6). A tetrahedron element consists of four subvolumes divided by four control surfaces. This model defines a function $F(x, y, z, t)$ that is greater than a critical value F_c wherever the filling fluid is present and smaller than F_c elsewhere (the pseudo-fluid). The function F is conveyed using the velocity field provided by the solution of the Navier–Stokes equations. The VOF transport equation can be written as:

$$\frac{\partial F}{\partial t} + u\frac{\partial F}{\partial x} + v\frac{\partial F}{\partial y} + w\frac{\partial F}{\partial z} = 0 \tag{42}$$

with the following initial and boundary conditions:

$$F(x, y, z, t) = 1 \text{ at the inlet} \tag{43}$$

$$F(x, y, z, t) = 0 \quad \text{at } t = 0 \tag{44}$$

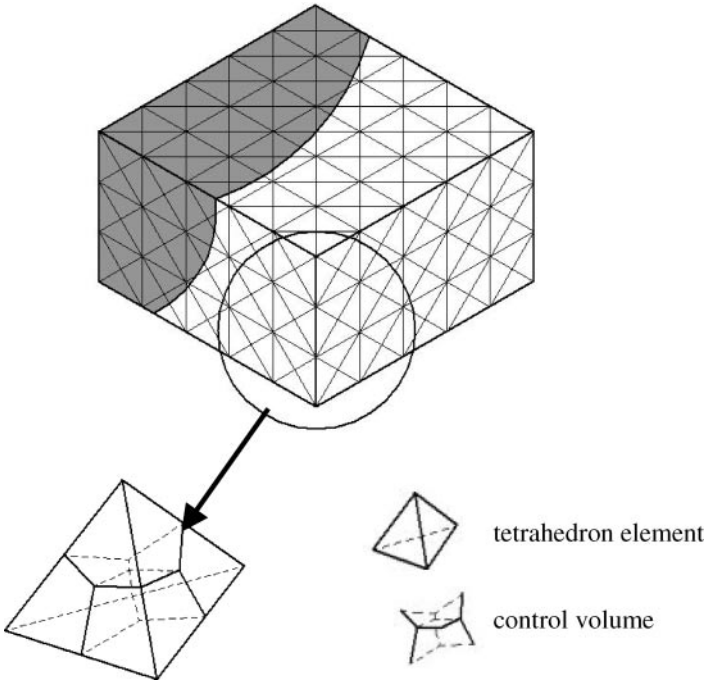

Figure 6. *Control volume for flow front advancing technique on 3D simulation.*

The hyperbolic Equation (42) is solved with the element by element technique of Lesaint and Raviart.

Since the Navier–Stokes equations are solved on the whole computational domain and because the pseudo-fluid has to exit the cavity freely, boundary conditions imposed on the cavity walls have to change dynamically. Depending on the values of F on the walls, the boundary conditions must satisfy the following conditions:

$$u = v = w = 0 \quad \text{when} \quad F \geq F_c \,(\text{Filled}) \tag{45}$$

$$\vec{\sigma} \cdot \vec{n} - \vec{p} \cdot \vec{n} = 0 \quad \text{when} \quad F < F_c \,(\text{Empty}) \tag{46}$$

$\vec{\sigma}$ is the extra-stress tensor. $\vec{n}$ is the normal vector and $\vec{p}$ is the pressure. These boundary conditions are imposed using an augmented Lagrangian technique.

SOLID–LIQUID INTERFACE TRACKING (ENTHALPY MODEL)

Figure 7 shows that the solid–liquid interface in an element predicted according to the enthalpy model. With the enthalpy model, the solid–liquid interface is calculated directly and it is clearly bounded. With the apparent heat capacity model, there is a mushy range of solid–liquid interface. The solid–liquid interface is assumed at the midline (or surface) of the mushy region [10].

Midplane Simulation (Hele-Shaw Model)

Temperature Field (Finite Difference Method, FDM)

A finite-difference representation of the transient and conduction terms in (21) is straightforward.

Pressure Field (Finite Element Method, FEM)

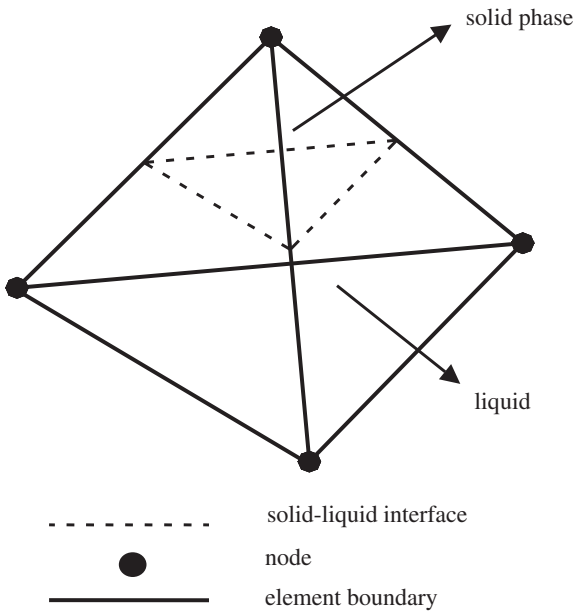

Figure 7. *Typical element presenting a position of the solid–liquid interface.*

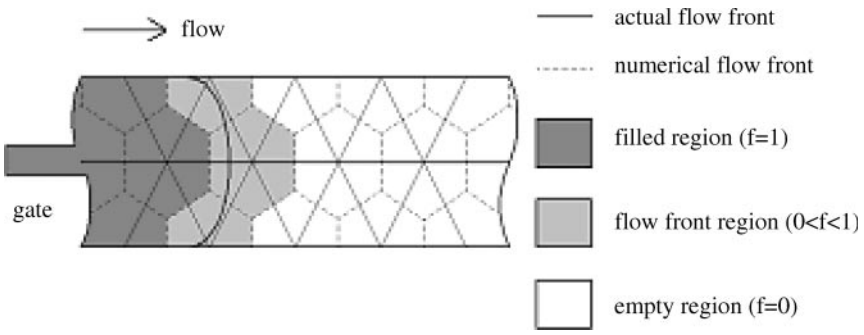

Figure 8. *Control volume for flow front advancing technique on midplane simulation.*

Once the temperature field within the computational domain is known at a given instant, the flow field and corresponding pressure distribution can be used the finite element method.

$$\int_{\Omega} \bar{w}_N \nabla \cdot (\tilde{S} \nabla p) d\Omega = \int_{\Omega} \left(G \frac{\partial p}{\partial t} + F \right) \bar{w}_N d\Omega \tag{47}$$

$\bar{w}_N$ is the weighting function and Ω is the flow domain.

Front Tracking

Figure 8 shows that the moving interface on control volume for midplane simulation.

(1) filled region: node for which the associated control volume is completely filled with polymer melt ($f = 1$); (2) flow front region: node whose control volume is partially filled with polymer melt ($0 < f < 1$); (3) empty region: node whose control volume has not yet been reached by the melt ($f = 0$).

The details of simulation of Hele-Shaw model are referenced on [11,12].

The mesh of 3D numerical simulation is shown on Figure 9. The numbers of element are 186441 and the numbers of node are 37678. The IBM PC is used to simulate the each case, The CPU is Pentium-4 2 GB, the RAM is 785 MB and the hard disk is 60 GB. The work time of each simulation wastes 59 min.

RESULTS AND DISCUSSION

Figure 10 shows that the short shot situation of experiment and the melt front shape between 3D numerical simulation and midplane numerical simulation on filling stage. Figure 10 shows that the initial shape of melt front is semicircle. When the melt front touches the right side edge, the shape of melt front indicates the 1/4 circle. At last, the melt front touches the left side edge, the shape of melt front shows the line shape. Whether the experiment, 3D, and midplane numerical simulation, the results seem to be the same. But there are differences between experiment, 3D, and midplane numerical simulation.

In Figure 10(a), the shape of melt front is semicircle whether experiment, 3D, and midplane numerical simulation. The shape of melt front between experiment and 3D numerical simulation is more concave upward than midplane numerical simulation on top side edge. In Figure 10(b), the shape of melt front seems to the same whether experiment, 3D, and midplane numerical simulation. The shape of melt front between experiment and 3D numerical simulation is more circular than midplane numerical simulation on top and

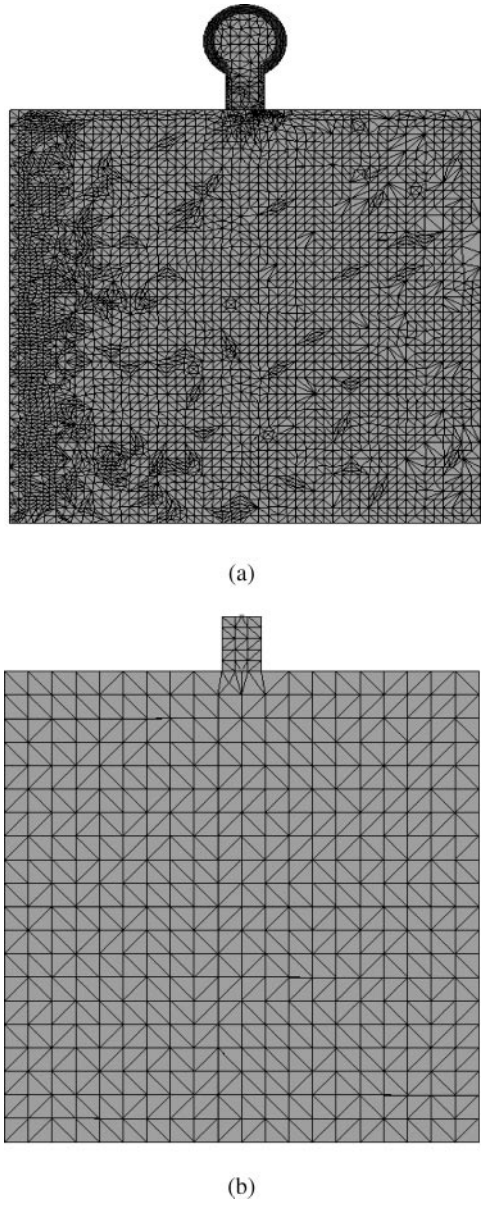

Figure 9. *(a) Mesh of 3D simulation; (b) Mesh of midplane simulation.*

right side edge. In Figure 10(c), the shape of melt front like 1/4 circle whether experiment, 3D, and midplane numerical simulation. The shape of melt front between experiment and 3D numerical simulation is more rounder than midplane numerical simulation on left and right side edge. In Figure 10(d), the shape of melt front between experiment and 3D numerical simulation is more straighter than midplane numerical simulation. The results of melt front of 3D numerical simulation are closed to experiment on Figure 10. The shape of melt front of midplane numerical simulation overestimates on filling stage. The midplane numerical simulation is based on Hele-Show model. It considers the velocity of

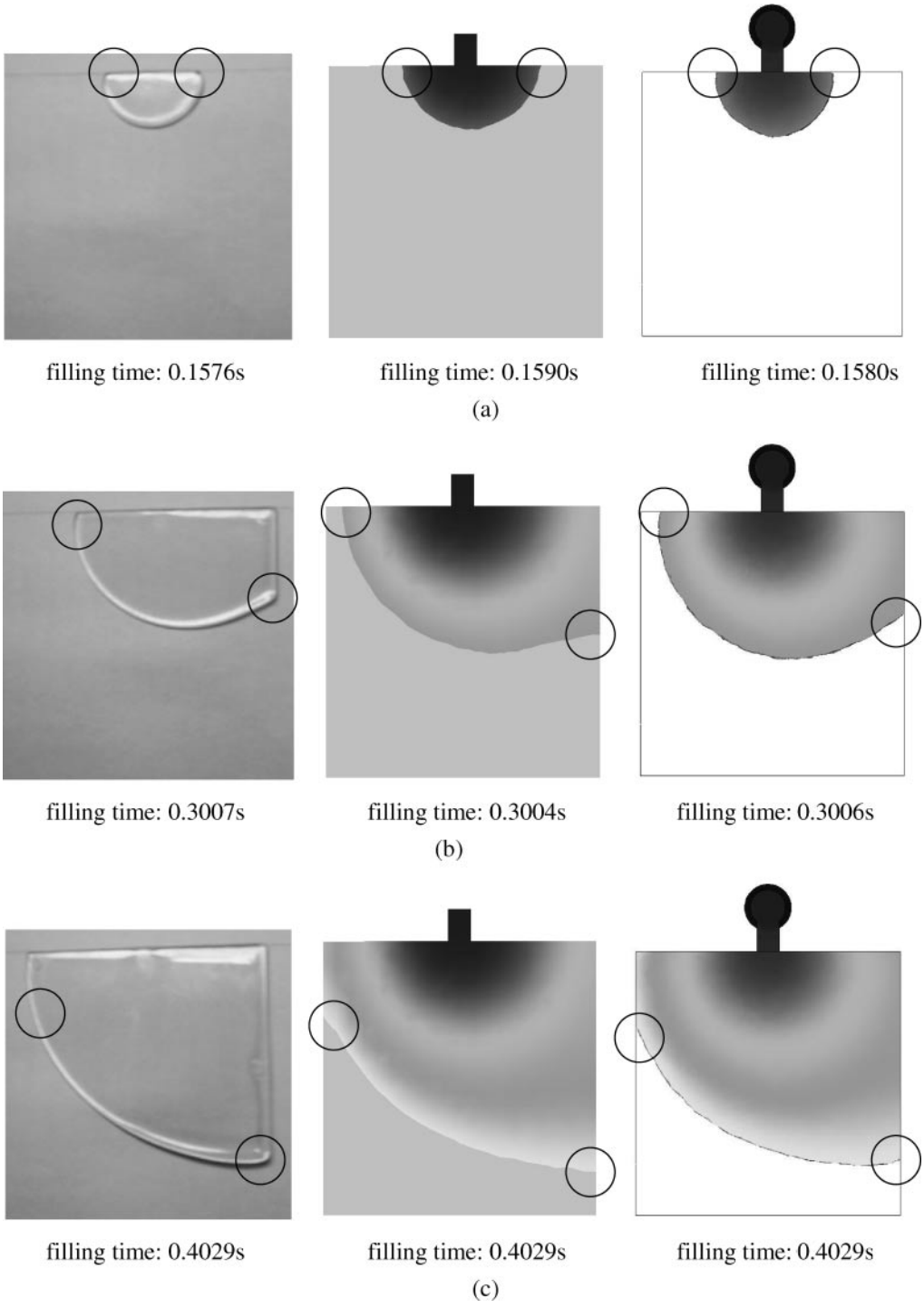

Figure 10. *The comparison of the results of experiment (left), 3D simulation (right) and midplane simulation (middle) for filling stage of injection molding.*

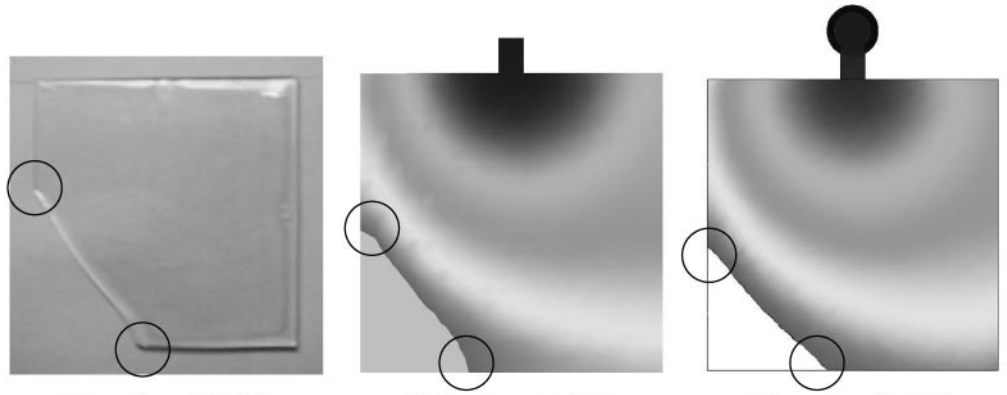

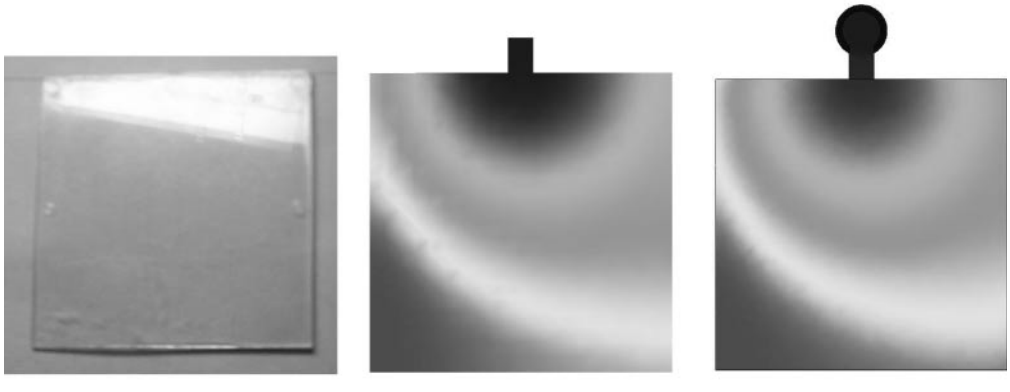

Figure 10. *Continued.*

x–y plane. The velocity (u, v) is function of z (thickness) direction. The no-slip boundary condition on the mold wall is just used for z (thickness) direction and it cannot consider the x–y plane. The 3D numerical simulation uses the real x, y, z coordinate of 3D model. The no-slip boundary condition of mold wall considers the x, y, z direction. The error of melt front of midplane numerical simulation near the side edge is larger than the experiment and 3D numerical simulation. The midplane numerical simulation is not simulated well on side edge of mold.

Figure 11 shows that the predicted point of solid layer thickness on lightguide plate. The point A, B, C are located on thick, middle, and thin region of lightguide plate. Figure 12 shows that the distribution of solid layer thickness on 3D and midplane numerical simulation from Figure 10. This figure indicates that the solid layer thickness increases when the filling time increases whether the thick, middle, or thin region on lightguide plate. The solid layer thickness of thick region is larger than middle region, than thin region on the same filling time. Figure 13 shows that the temperature distribution on thickness direction of lightguide plate. The temperature of thick region is

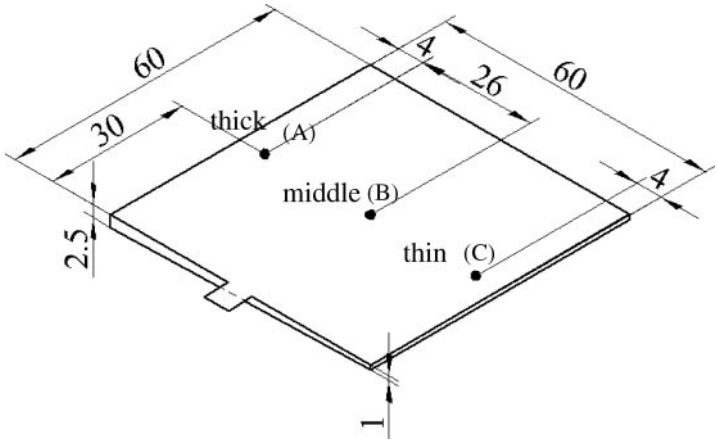

Figure 11. *The predicted point of solid layer thickness.*

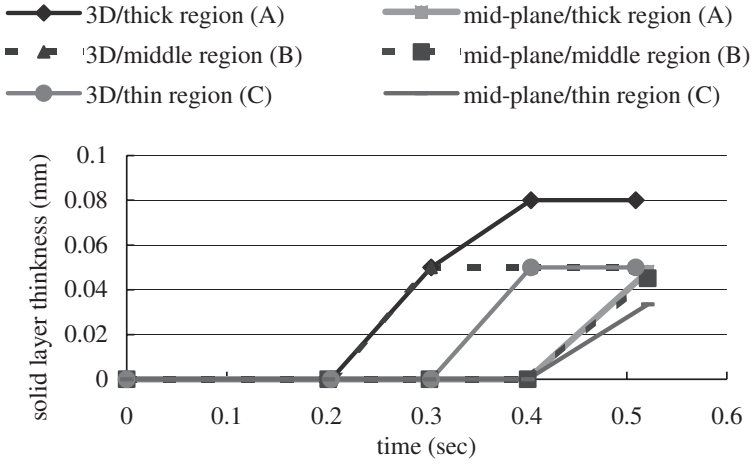

Figure 12. *The solid layer thickness of different region for 3D and midplane simulation.*

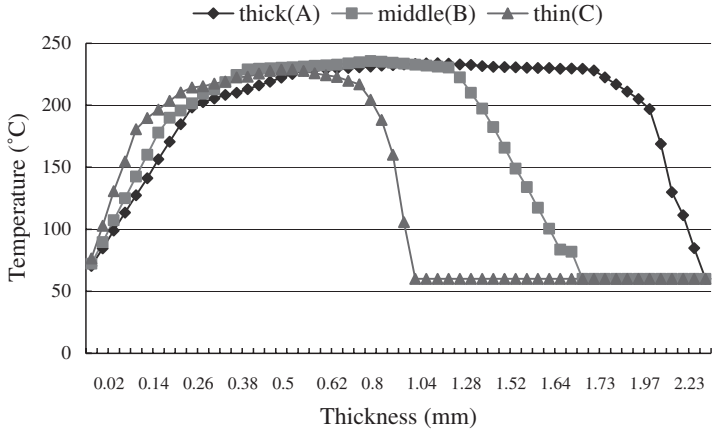

Figure 13. *Temperature distribution of thickness direction of light guide plate.*

higher than middle region, than thin region. Because the time of high temperature region cooling to glass transition temperature is slower than the other region, the solid layer thickness of thick region is larger than the other region. Figure 14 shows the solid layer thickness of different regions at the end of filling time. The thickness of thick region is 0.8 mm, the middle, and thin region is 0.5 mm. Because the solid layer borns, the thickness of mold becomes thinner. The thickness of thin region of the mold has just 0.5 mm to let the melt flow and the thickness of thick region of the mold has just 1.3 mm to let the melt flow. The flow resistance is higher on thin region, the melt flow can easily fill to the thick region.

Figure 15 shows that the comparison of pressure distribution on thick and thin region for 3D simulation, experiment, and midplane simulation on filling stage of injection molding. Whether experiment or numerical simulation (3D, midplane), the pressure distribution of thick region is higher than thin region on the same filling time. When the plastic melt flows into the thin region, the plastic melt is easily squeezed by mold wall that induces the melt temperature to increase. This situation causes the melt viscosity to decrease so that the injection pressure lessens. Whether thick region or thin region, the pressure distribution of 3D numerical simulation is larger than midplane simulation. The pressure distribution of 3D numerical simulation is closer to the experiment in Figure 15.

The results show that the melt front of 3D numerical simulation is similar to the experiment. The results also show that the pressure distribution of 3D numerical simulation is closer to the experiment. The error of midplane numerical simulation is large on filling stage of injection molding. To sum up, the melt front shape and pressure distribution is very closer between 3D numerical simulation and experiment on injection mold filling.

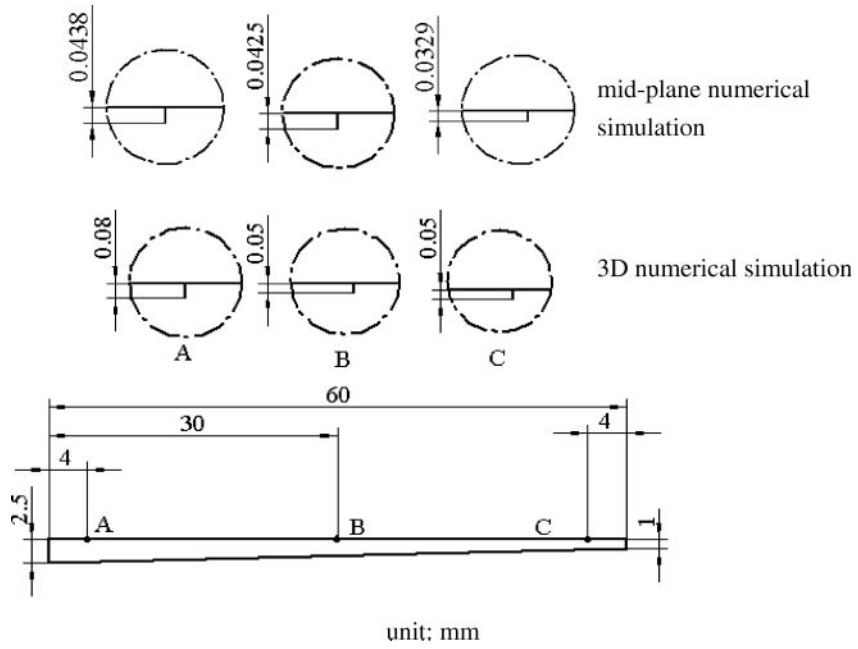

Figure 14. *Solid layer thickness on the end of filling stage for 3D and midplane simulation.*

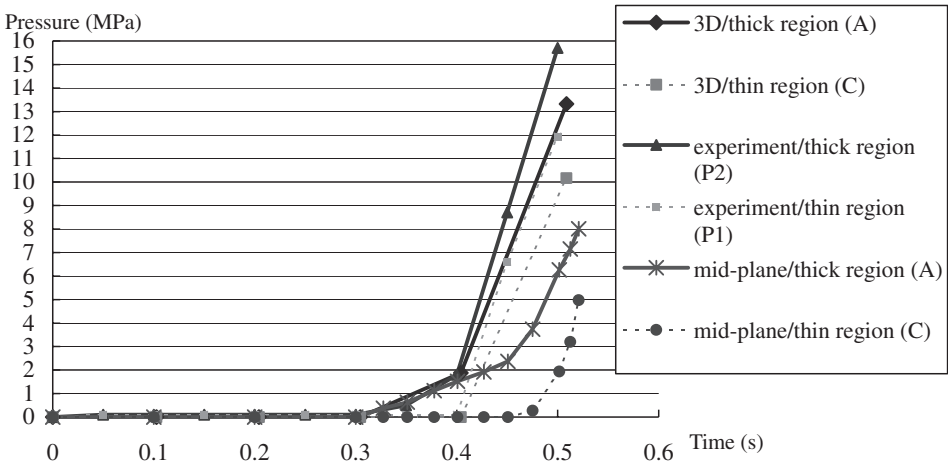

Figure 15. *Pressure distribution of experiment, 3D simulation and midplane simulation.*

CONCLUSIONS

Optical product is very popular at present. The development of injection machine, the establishment of processing conditions and mold design is lack of references. This paper indicates that the melt front and pressure distribution of 3D numerical simulation is closer to experiment. The position of melt front on midplane numerical simulation overestimates compared with experiment and 3D numerical simulation. The pressure distribution of midplane numerical simulation is smaller than experiment and 3D numerical simulation. To sum up, the melt front and pressure distribution of midplane numerical simulation produces the trouble especially on the side wall of mold on filling stage of injection molding.

BIOGRAPHIES

Y. K. Shen

Y. K. Shen received his PhD degree in the School of Navy Architecture and Ocean Engineering from the National Taiwan University, Taipei, Taiwan, ROC. He is an Associate Professor in the Department of Mechanical Engineering, Lunghwa University of Science and Technology, Taoyuan, Taiwan, ROC. His research is in the areas of micro-injection molding, flip chip package, and moldflow analysis.

S. Y. Yang

S. Y. Yang received his PhD degree in the School of Mechanical Engineering from the University of Minnesota, Minneapolis, USA. He is a Professor in the Department of Mechanical Engineering, National Taiwan University, Taipei, Taiwan, ROC. His research is in the areas of micro-injection molding, gas-assisted injection molding, and hot embossing molding.

C-C. A. Chen

C-C. A. Chen received his PhD degree in the School of Mechanical Engineering from the University of Wisconsin, Madison, USA. He is an Associate Professor in the Department of Mechanical Engineering, National Taiwan University of Science and Technology, Taipei, Taiwan, ROC. His research is in the areas of micro-injection molding, micro turning, and micro abrasive machining.

W. Y. Wu

W. Y. Wu is a graduate student in the School of Mechanical Engineering, Lunghwa University of Science and Technology.

H. M. Jian

H. M. Jian is a graduate student in the School of Mechanical Engineering, National Taiwan University.

REFERENCES

1. Zachert, J. and Michaeli, W. (1998). *J. Reinf. Plast. Compos.*, **17**(10): 955–962.
2. Floryan, J.M. and Rusmussen, H. (1989). *Appl. Mech. Rev.*, **42**(12): 323–341.
3. Shen, Y.K. and Wu, W.Y. (2002). *Int. Commun. Heat Mass Transf.*, **29**(3): 423–431.
4. Hetu, J.F., Gao, D.M., Garcia-Rejon, A. and Salloun, G. (1998). *Polym. Eng. Sci.*, **38**(2): 223–236.
5. Kabanemi, K.K., Hetu, J.F. and Garcia-Rejon, A. (1997). *International Polymer Processing*, **II**(2): 182–191.
6. Haagh, G.A.A.V. and Van De Vosse, F.N. (1998). *Int. J. Numer. Methods Fluids*, **28**: 1355–1369.
7. Hwang, C.J. and Kwon, T.H. (2002). *Polym. Eng. Sci.*, **42**(1): 33–50.
8. Shen, Y.K. (2001). *Int. Commun. Heat Mass Transf.*, **28**(1): 139–148.
9. Harlow, F.H. and Welch, J.E. (1956). *Phys. Fluids*, **8**(12): 2182–2189.
10. Li, C.S., Hung, C.F. and Shen, Y.K. (1995). *Int. Commun. Heat Mass Transf.*, **22**(2): 167–177.
11. Kennedy, P. (1993). *Flow Analysis Reference Manual*, Hanser Publishers, New York.
12. Wang, V.W., Hieber, C.A. and Wang, K.K. (1986). *J. Polym. Eng.*, **7**(1): 21–45.